

Spin dynamics in the antiferromagnetic phase of electron-doped cuprate superconductors

Qingshan Yuan,^{1,2} T. K. Lee,³ and C. S. Ting¹

¹*Texas Center for Superconductivity and Advanced Materials and
Department of Physics, University of Houston, Houston, TX 77204*

²*Pohl Institute of Solid State Physics, Tongji University, Shanghai 200092, P. R. China*

³*Institute of Physics, Academia Sinica, Nankang, Taipei, Taiwan 11529*

Based on the t - t' - t'' - J model we have calculated the dynamical spin susceptibilities in the antiferromagnetic (AF) phase for electron-doped cuprates, by use of the slave-boson mean-field theory and random phase approximation. Various results for the susceptibilities versus energy and momentum have been shown at different dopings. At low energy, except the collective spin-wave mode around (π, π) and 0, we have primarily observed that resonance peaks will appear around $(0.3\pi, 0.7\pi)$ and equivalent points with increasing doping, which are due to the single particle-hole excitations between the two AF bands. The peaks are pronounced in the transverse susceptibility but not in the longitudinal one. These features are predicted for neutron scattering measurements.

PACS numbers: 74.72.Jt, 71.10.Fd, 74.25.Ha

Since their discovery the hole- and electron-doped high- T_c cuprate superconductors have been noticed to exhibit many different properties. This is immediately seen from the phase diagram in the temperature/doping plane. In hole-doped compounds, e.g., $\text{La}_{2-x}\text{Sr}_x\text{CuO}_4$, the antiferromagnetic (AF) order stabilizes only in a narrow doping region $x \leq 0.02$,¹ whereas it persists up to $x = 0.14$ in electron-doped ones, e.g., $\text{Nd}_{2-x}\text{Ce}_x\text{CuO}_4$.² The electron-hole asymmetry has also been observed in various measurements such as nuclear magnetic resonance,³ inelastic neutron scattering,⁴ etc. Particularly, recent angle-resolved photoemission spectroscopy (ARPES) experiments^{5,6} have revealed the peculiar Fermi surface (FS) structure in electron-doped cuprate $\text{Nd}_{2-x}\text{Ce}_x\text{CuO}_4$. It was found that at low doping the FS is a small pocket centered at $(\pi, 0)$, in contrast to the hole-doped case⁷ where it is around $(\pi/2, \pi/2)$. Moreover, upon increased doping another pocket begins to form around $(\pi/2, \pi/2)$ and eventually at optimal doping $x = 0.15$ the several FS pieces together constitute a large curve around (π, π) .

Theoretically, the essential role of the next nearest neighbor (n.n.) hopping t' has been pointed out to understand the electron-hole asymmetry.^{8,9} By inclusion of t' and possibly the third n.n. hopping t'' in two types of models t - J and t - U , numerous numerical and analytical studies have been carried out to explore the different properties of electron-doped cuprates.^{10,11,12,13,14,15,16,17} Much attention has been paid to the interpretation^{14,15,16,17} of the FS evolution with doping as observed by ARPES.^{5,6} By use of the t - t' - t'' - U model Kusko *et al.*¹⁴ have derived the mean-field (MF) quasiparticle energy bands in the AF state. In order to get the consistent results with ARPES, however, they need to introduce a doping-dependent effective parameter U , see also Ref. [16]. Alternatively, we have adopted the t - t' - t'' - J model to construct the FS.¹⁷ The use of t - J -type models for the electron-doped cuprates is a natural generalization from their extensive application

to the hole-doped ones, and is largely stimulated by the accumulating evidence for the universal d -wave superconducting (SC) gap¹⁸ in both kinds of materials. Without phenomenological parameters as argued by Kusko *et al.*, we have obtained that at low doping only one AF band is crossed by the Fermi level around $(\pi, 0)$, and upon increased doping the other one will again be crossed around $(\pi/2, \pi/2)$. Correspondingly a FS pocket forms initially around $(\pi, 0)$ and later the new one appears around $(\pi/2, \pi/2)$, in agreement with the ARPES data.

In view of the sample quality, on the other hand, it may be questioned whether the multiple pockets around the inequivalent points revealed by ARPES are detected from the uniform phase of the whole sample or from the different regions of the inhomogeneous sample. Thus other experimental measurements complementary to ARPES are strongly needed. Naturally, any theoretical prediction based on the current result will be useful to guide the experiments. For this purpose the spin dynamics, which can be measured by inelastic neutron scattering, is calculated in this paper. If it is really true that the new FS emerges in the same uniform phase with the old one upon increased doping, the novel particle-hole (p - h) excitations between them should lead to characteristic features for the spin dynamics which implies the information of the spin/charge excitations.

At present, the calculations on the dynamical spin susceptibilities for electron-doped cuprates^{12,13,19} are very limited, and mostly done in the SC and normal states. Here we will concentrate on the AF phase, and study the variation of the susceptibilities with doping which has not yet been investigated. The significance of the topic is highlighted in the electron-doped materials because the AF phase is robust to survive a wide doping range and the understanding of its nature becomes crucial. Thus our motivation is twofold. On one hand, we wish to predict some characteristic results for experimental verification. On the other hand, we perform the

general formulation of the dynamical spin susceptibilities under the background of the AF order, which is rarely presented in the literature.²⁰ The random phase approximation (RPA) is used to take the spin fluctuation into account. Our main result is that with increasing doping new resonance peaks will appear at low energy around $(0.3\pi, 0.7\pi)$ and equivalent points, which are pronounced in the transverse susceptibility but not in the longitudinal one.

We begin with the t - t' - t'' - J model Hamiltonian

$$H = -t \sum_{\langle ij \rangle \sigma} (c_{i\sigma}^\dagger c_{j\sigma} + \text{h.c.}) - t' \sum_{\langle ij \rangle 2\sigma} (c_{i\sigma}^\dagger c_{j\sigma} + \text{h.c.}) - t'' \sum_{\langle ij \rangle 3\sigma} (c_{i\sigma}^\dagger c_{j\sigma} + \text{h.c.}) + J \sum_{\langle ij \rangle} (\mathbf{S}_i \cdot \mathbf{S}_j - \frac{1}{4} n_i n_j) - \mu_0 \sum_{i\sigma} c_{i\sigma}^\dagger c_{i\sigma}, \quad (1)$$

where all the notation is standard. For electron-doping, one has $t < 0$, $t' > 0$ and $t'' < 0$.^{8,9,10,11} Throughout the work $|t|$ is taken as the energy unit. Typical values are adopted: $t' = 0.3$, $t'' = -0.2$ and $J = 0.3$.

We treat the Hamiltonian (1) by the slave-boson MF theory. Without details we briefly introduce the necessary formulas. Under assumption of boson condensation and definition of MF parameters: the staggered magnetization $m = (-1)^i \langle S_i^z \rangle$ and the uniform bond order $\chi = \langle f_{i\sigma}^\dagger f_{j\sigma} \rangle$ (f : spinon operator), the Hamiltonian (1) is decoupled as follows in momentum space¹⁷

$$H_M = \sum'_{k,\sigma} (\varepsilon_k f_{k\sigma}^\dagger f_{k\sigma} + \varepsilon_{k+Q} f_{k+Q\sigma}^\dagger f_{k+Q\sigma}) - 2Jm \sum'_{k,\sigma} \sigma (f_{k\sigma}^\dagger f_{k+Q\sigma} + \text{h.c.}) + 2NJ(\chi^2 + m^2), \quad (2)$$

where $\varepsilon_k = (2|t|x - J\chi)(\cos k_x + \cos k_y) - 4t'x \cos k_x \cos k_y - 2t''x(\cos 2k_x + \cos 2k_y) - \mu$ (x : doping concentration), $Q = (\pi, \pi)$, and N is the total number of lattice sites. \sum'_k means the summation over only the magnetic Brillouin zone (MBZ): $-\pi < k_x \pm k_y \leq \pi$. Above, the local constraint for no double occupancy has been treated in average as usually done. In addition, we do not consider the potential pairing in order to harmonize with the experimental observation for the large range of pure AF phase.

By use of the unitary transformations: $f_{k\sigma} = \cos \theta_k \alpha_{k\sigma} + \sigma \sin \theta_k \beta_{k\sigma}$ and $f_{k+Q\sigma} = -\sigma \sin \theta_k \alpha_{k\sigma} + \cos \theta_k \beta_{k\sigma}$ [$\sigma = \uparrow$ (+) or \downarrow (-)], where $\cos 2\theta_k = (\varepsilon_{k+Q} - \varepsilon_k)/\gamma_k$, $\sin 2\theta_k = -4Jm/\gamma_k$ and $\gamma_k = \sqrt{(\varepsilon_{k+Q} - \varepsilon_k)^2 + (4Jm)^2}$, the Hamiltonian (2) can be diagonalized in terms of $\alpha_{k\sigma}$ and $\beta_{k\sigma}$, with the two energy bands $\xi_{k,\alpha} = (\varepsilon_k + \varepsilon_{k+Q} - \gamma_k)/2$ and $\xi_{k,\beta} = (\varepsilon_k + \varepsilon_{k+Q} + \gamma_k)/2$.

For each given doping x and temperature T , the MF parameters m and χ , as well as the chemical potential μ are calculated self-consistently. Then the energy bands and the corresponding FS can be plotted in the MBZ. All the results have been shown in Ref. [17] for $T = 10^{-3}$. Mainly, with increasing doping the two AF bands become close to each other due to the decreasing magnetization. Within a very narrow doping range around $x = 0.144$ they are both crossed by the Fermi level around $(\pi, 0)$ (and equivalent points) and $(\pm\pi/2, \pm\pi/2)$, respectively, leading to multiple FS pockets around the inequivalent points. In order to reveal their consequence to the observable physical quantities, we calculate the spin dynamics in the following.

The spin susceptibilities (transverse and longitudinal) are defined by

$$\chi_{(0)}^{+- (zz)}(q, q', \tau) = +\frac{1}{N} \langle T_\tau S_q^{+(z)}(\tau) S_{-q'}^{-(z)}(0) \rangle_{(0)}, \quad (3)$$

where $\langle \dots \rangle_{(0)}$ means thermal average on the eigenstates of $H_{(M)}$, $S_q^+ = \sum_i S_i^+ e^{iq \cdot R_i} = \sum_k f_{k+q}^\dagger f_{k\downarrow}$, $S_q^- = (S_{-q}^+)^{\dagger}$ and $S_q^z = \frac{1}{2} \sum_{k\sigma} \sigma f_{k+q\sigma}^\dagger f_{k\sigma}$. Correspondingly the term $J \sum_{\langle ij \rangle} \mathbf{S}_i \cdot \mathbf{S}_j$ is rewritten as $(1/N) \sum_q J(q) (S_q^+ S_{-q}^- + S_q^z S_{-q}^z)$ with $J(q) = J(\cos q_x + \cos q_y)$.

We first calculate $\chi_0^{+- (zz)}$ under the quadratic Hamiltonian H_M . By transforming f operator into α and β ones we finally obtain

$$\chi_0^{+-}(q, q', i\omega_n) = \delta_{q',q} \chi_0^{+-}(q, i\omega_n) + \delta_{q',q+Q} \chi_0^{+-}(q, q+Q, i\omega_n), \quad (4)$$

$$\chi_0^{zz}(q, q', i\omega_n) = \delta_{q',q} \chi_0^{zz}(q, i\omega_n), \quad (5)$$

where

$$\chi_0^{+-}(q, i\omega_n) = -\frac{1}{N} \sum'_k [\cos^2(\theta_k + \theta_{k+q})(F_{\alpha\alpha} + F_{\beta\beta}) + \sin^2(\theta_k + \theta_{k+q})(F_{\alpha\beta} + F_{\beta\alpha})], \quad (6)$$

$$\chi_0^{+-}(q, q+Q, i\omega_n) = \frac{1}{2N} \sum'_k [(\sin 2\theta_{k+q} - \sin 2\theta_k)(F_{\alpha\alpha} - F_{\beta\beta}) + (\sin 2\theta_{k+q} + \sin 2\theta_k)(F_{\alpha\beta} - F_{\beta\alpha})], \quad (7)$$

$$\chi_0^{zz}(q, i\omega_n) = -\frac{1}{2N} \sum'_k [\cos^2(\theta_k - \theta_{k+q})(F_{\alpha\alpha} + F_{\beta\beta}) + \sin^2(\theta_k - \theta_{k+q})(F_{\alpha\beta} + F_{\beta\alpha})] \quad (8)$$

with abbreviations

$$F_{\eta\eta'} = \frac{n(\xi_{k+q,\eta}) - n(\xi_{k,\eta'})}{i\omega_n + \xi_{k+q,\eta} - \xi_{k,\eta'}} \quad (\eta, \eta' = \alpha, \beta).$$

Above ω_n are Matsubara frequencies and $n(\dots)$ is the Fermi function. Since the eigenstates of H_M exhibit the AF order that breaks the spin rotational symmetry, the simple relation $\chi_0^{+-} = 2\chi_0^{zz}$ which holds in the case of $m = 0$ is no longer valid. Moreover, the nondiagonal correlation function χ_0^{+-} with $q' = q + Q$ [Eq. (7)] arises due to the umklapp processes. It is instructive to have a look at the physics implied by the diagonal functions $\chi_0^{+-(zz)}(q, i\omega_n)$ from the above Eqs. (6) and (8). With momentum transfer q there are two types of p - h excitations, either within the single band (α or β) as described by $F_{\alpha\alpha}$ and $F_{\beta\beta}$ or between the two bands by $F_{\alpha\beta}$ and $F_{\beta\alpha}$. We notice that the two, intraband and

interband p - h excitations, have different weights in their contribution to $\chi_0^{+-(zz)}(q, i\omega_n)$. Also, the difference between $\chi_0^{+-}(q, i\omega_n)$ and $\chi_0^{zz}(q, i\omega_n)$ exists in their different weighing factors for each type of excitations. If we consider low temperature ($T \rightarrow 0$) and low energy transfer ($\omega \rightarrow 0$), the dominant contribution to $\chi_0^{+-(zz)}(q, i\omega_n)$ comes from those excitations within the very vicinity of the FS. Thus we expect that new resonance peaks with large momentum transfer will arise with increasing doping due to the emergence of the new FS pockets around $(\pm\pi/2, \pm\pi/2)$.

We further calculate $\chi^{+-(zz)}(q, q', i\omega_n)$. The residual fluctuation of the J -term beyond MF is considered by the RPA. We have obtained the similar equations for $\chi^{+-(zz)}(q, q', i\omega_n)$ to Eqs. (4) and (5) for $\chi_0^{+-(zz)}(q, q', i\omega_n)$, with correspondingly

$$\chi^{+-}(q, i\omega_n) = \frac{\chi_0^{+-}(q, i\omega_n) - J(q+Q)[\chi_0^{+-}(q+Q, q, i\omega_n)\chi_0^{+-}(q, q+Q, i\omega_n) - \chi_0^{+-}(q, i\omega_n)\chi_0^{+-}(q+Q, i\omega_n)]}{[1 + J(q)\chi_0^{+-}(q, i\omega_n)][1 + J(q+Q)\chi_0^{+-}(q+Q, i\omega_n)] - J(q)J(q+Q)\chi_0^{+-}(q+Q, q, i\omega_n)\chi_0^{+-}(q, q+Q, i\omega_n)}, \quad (9)$$

$$\chi^{+-}(q, q+Q, i\omega_n) = \frac{\chi_0^{+-}(q, q+Q, i\omega_n)}{\text{denominator of Eq. (9)}}, \quad (10)$$

$$\chi^{zz}(q, i\omega_n) = \frac{\chi_0^{zz}(q, i\omega_n)}{1 + J(q)\chi_0^{zz}(q, i\omega_n)}. \quad (11)$$

The formula for $\chi^{+-}(q, i\omega_n)$ becomes complicated due to the existence of the nondiagonal χ_0^{+-} . As a result, it may contain a pole, which corresponds to a collective spin-wave excitation mode. The imaginary part of $\chi^{+-}(q, i\omega_n)|_{i\omega_n \rightarrow \omega + i\Gamma}$ is shown by Fig. 1 as a function of ω for various q vectors. Throughout the calculation we have taken $T = 10^{-3}|t|$, the damping rate $\Gamma = 0.01|t|$, and 500×500 k points in the MBZ. Three typical doping values are adopted in Fig. 1: small $x = 0.04$, medium $x = 0.1$ and $x = 0.144$ where new FS pockets around $(\pm\pi/2, \pm\pi/2)$ appear. Globally it is seen that with increasing doping the visible susceptibility spans a wider energy range, due to the broadening bandwidth and reducing AF gap. For details, we first look at the region $q \rightarrow Q = (\pi, \pi)$ shown by the several lower panels of Figs. 1(c) and 1(d). It is observed that a sharp peak, particularly for doping $x = 0.04$ (note three times reduction of the amplitude in this case), is formed and becomes stronger when q is closer to Q . The peak position in each panel is around the magnon excitation energy for the corresponding Heisenberg model as shown by the cross on the abscissa. This indicates the collective spin-wave excitation in the presence of carriers. The peak is more prominent for $x = 0.04$ because the collective mode is better defined for smaller doping. Similarly, the peak

from the spin-wave excitation is present at low energy when $q \rightarrow 0$, as seen from the several upper panels of Fig. 1(a).

Then we come to q away from Q and 0. Now the collective excitation has a sizable energy. We notice that this mode may not always be exhibited by the RPA, for example, in the line: $q_x + q_y = \pi$ one has $\chi^{+-} = \chi_0^{+-}$ because of $J(q) = 0$. However, our interest is the experimentally relevant low-energy region where the single p - h excitations play the essential role when q is away from Q and 0. A notable feature observed at low ω ($< 0.4J \sim 40$ meV) is that the susceptibility becomes finite when $x = 0.144$ for some wave vectors, e.g., $q = (0.3\pi, 0.7\pi)$ as shown in Fig. 1(b). To fully view the susceptibility in the whole q plane, we have fixed the low energy $\omega = 0.1J$ and plotted the density of $\text{Im}\chi^{+-}(q, \omega)$ in Fig. 2. There is a huge peak around Q in each panel which has been left blank. With increasing doping, except an expansion of the blank region indicating the broadening of the peak around Q , we can observe the considerable intensity around the new wave vectors $q/2\pi \simeq (0.15, 0.37)$ and equivalent points [keep in mind the symmetry of $\chi^{+-(zz)}$ with respect to q : $q_x \leftrightarrow q_y$ or $q_{x(y)} \rightarrow -q_{x(y)} + 2\pi$]. To more clearly see the appearance of the new peaks, we have calculated $\text{Im}\chi^{+-}(q, \omega)$ vs q along a few lines in the q plane for different dopings, which are shown by Figs. 3(a) and 3(b). When x approaches 0.144, the primary feature is that new peaks grow rapidly around $q/2\pi \simeq (0.14, 0.36)$ and $(0.36, 0.14)$ as shown in Fig. 3(b). By checking the FS, see Fig. 3 in Ref. [17], we conclude that these peaks are in-

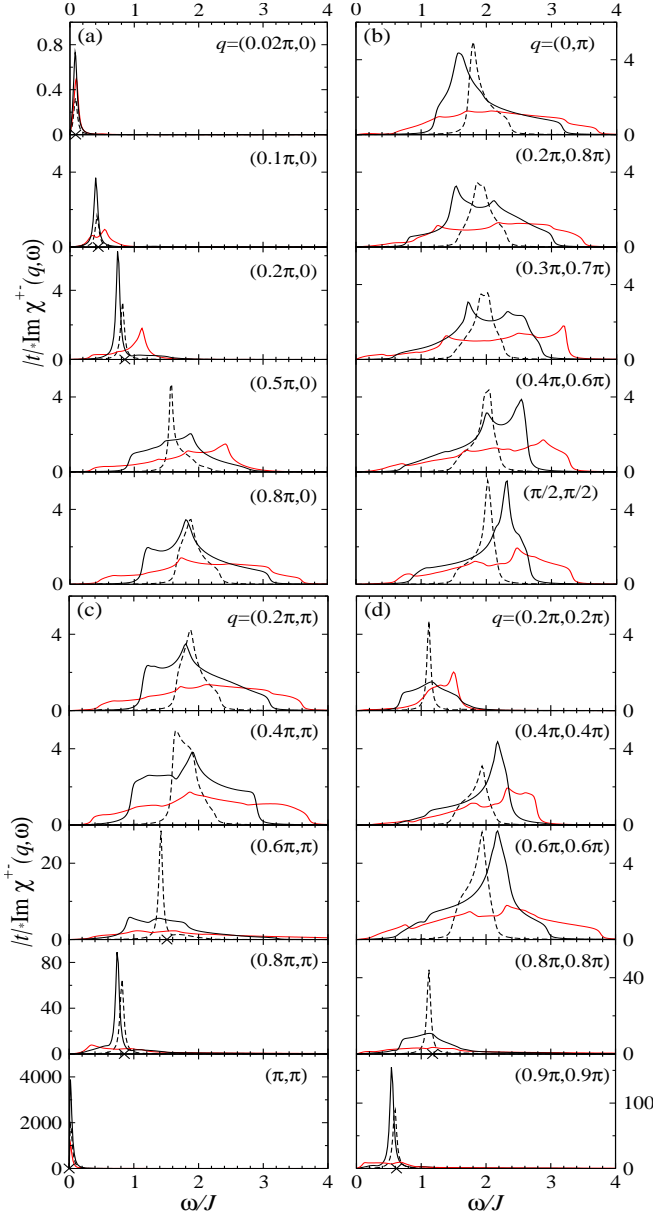


FIG. 1: The transverse dynamical susceptibility vs frequency for various wave vectors: (a) $q_y = 0$, (b) $q_x + q_y = \pi$, (c) $q_y = \pi$, and (d) $q_x = q_y$. The dashed, solid, and red lines in each panel represent the results for doping $\delta = 0.04, 0.1$, and 0.144 , respectively. Note that all the values for $\delta = 0.04$ have been reduced by three times. The crosses shown in part of the panels $q \rightarrow 0$ and Q denote the single magnon excitation energies for the Heisenberg model: $J\sqrt{4 - (\cos q_x + \cos q_y)^2}$. The parameters are: temperature $T = 10^{-3}$ and damping rate $\Gamma = 10^{-2}$ (in units of $|t|$).

duced by the interband excitations, e.g., from the pocket around $(-\pi, 0)$ contributed by the α band to that around $(-\pi/2, \pi/2)$ contributed by the β band. From Fig. 3(a), we also see that a hump around $q/2\pi = (0.5, 0)$ appears for $x = 0.144$, which is due to the intra- β -band excitations, e.g., from the FS pocket around $(-\pi/2, \pi/2)$ to the

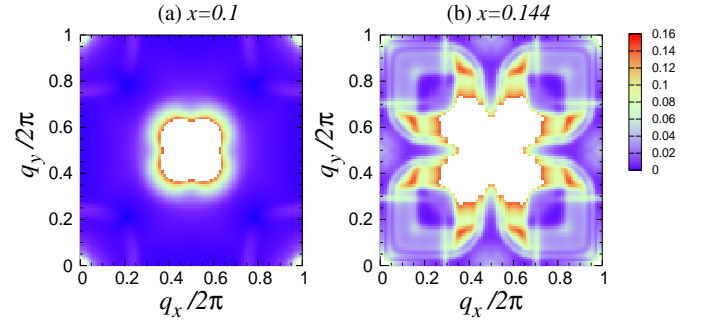


FIG. 2: The density plots of $\text{Im}\chi^{+-}(q, \omega)$ in the q plane for doping $x = 0.1$ and 0.144 , with fixed low energy $\omega = 0.1J$. The white region in each panel contains a huge peak around (π, π) originating from the collective spin-wave excitation, which is not plotted in order to highlight the much weaker peaks at other wave vectors. With increasing doping, new peaks around $q/2\pi \simeq (0.15, 0.37)$ and equivalent points are clearly seen.

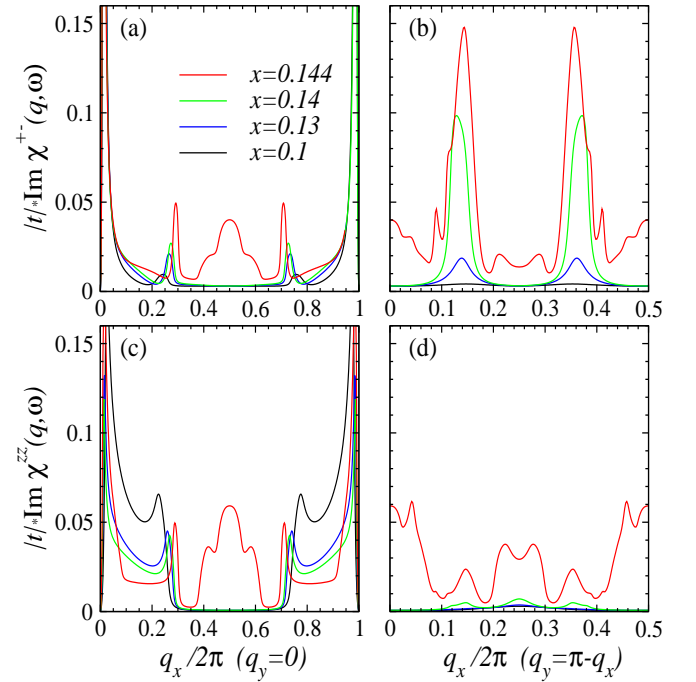


FIG. 3: $\text{Im}\chi^{+-}(q, \omega)$ [(a) and (b)] and $\text{Im}\chi^{zz}(q, \omega)$ [(c) and (d)] at $\omega = 0.1J$ with change of q along the lines: (i) $q_y = 0$ [(a) and (c)], (ii) $q_x + q_y = \pi$ [(b) and (d)].

one around $(\pi/2, \pi/2)$. Note that all the above new peaks are characteristic of the emergence of the new FS pockets (or the close proximity of the β band to the Fermi level). In addition, the peak seen in the region $0.2 < q_x/2\pi < 0.3$ in Fig. 3(a), which slightly moves with doping, comes from the intra- α -band excitations between the old pockets around $(\pi, 0)$ and $(-\pi, 0)$.

Similarly, we have calculated $\text{Im}\chi^{zz}(q, \omega)$ which is qualitatively the same as $\text{Im}\chi_0^{zz}(q, \omega)$ but quantitatively enhanced in most cases. A few results for the longitu-

dinal susceptibility at a fixed energy have been shown in Figs. 3(c) and 3(d), for a comparison with the corresponding transverse one. We notice that the primary peaks around $q/2\pi \simeq (0.14, 0.36)$ and $(0.36, 0.14)$ as seen in χ^{+-} upon increased doping become much weaker in χ^{zz} , and may even be screened by other peaks nearby.

Finally, we comment on the new peaks around $q/2\pi \simeq (0.14, 0.36)$ and equivalent points appearing in the transverse susceptibility. As mentioned above, they arise from the interband p - h excitations. From the FS plot, we do not see a nesting wave vector connecting two FS pockets which belong to the two bands, respectively. So the new peaks found here are not so strong, but in the same order as found in some similar calculations.²¹ They should be observable by neutron scattering which can have measured very weak intensity of the spin excitations.²² We point out that all the plots shown in Fig. 3 are qualitatively the same for any low energy $\omega/J < 0.4$, but the ordinates are enlarged with increasing ω . Thus the new

peaks may be enhanced by a larger ω , making their observation easier.

In conclusion, we have calculated the dynamical spin susceptibilities in the AF phase for the electron-doped t - t' - t'' - J model. Various results for the energy and momentum dependences have been given at different dopings. At low energy, except the collective spin-wave mode around (π, π) and 0, the primary observation is that new resonance peaks will appear around $(0.3\pi, 0.7\pi)$ and equivalent points with increasing doping, which are due to the interband p - h excitations. These peaks are pronounced in the transverse susceptibility but not in the longitudinal one. We hope that our theoretical results will stimulate the experimental measurements.

We thank F. Yuan for helpful discussions. This work was supported by the Texas Center for Superconductivity and Advanced Materials at the University of Houston and the Robert A. Welch Foundation.

-
- ¹ H. Takagi, T. Ido, S. Ishibashi, M. Uota, S. Uchida, and Y. Tokura, Phys. Rev. B **40**, 2254 (1989).
 - ² G. M. Luke, L. P. Le, B. J. Sternlieb, Y. J. Uemura, J. H. Brewer, R. Kadono, R. F. Kiefl, S. R. Kreitzman, T. M. Riseman, C. E. Stronach, M. R. Davis, S. Uchida, H. Takagi, Y. Tokura, Y. Hidaka, T. Murakami, J. Gopalakrishnan, A. W. Sleight, M. A. Subramanian, E. A. Early, J. T. Markert, M. B. Maple, and C. L. Seaman, Phys. Rev. B **42**, 7981 (1990).
 - ³ G.-q. Zheng, T. Sato, Y. Kitaoka, M. Fujita, and K. Yamada, Phys. Rev. Lett. **90**, 197005 (2003).
 - ⁴ K. Yamada, K. Kurahashi, T. Uefuji, M. Fujita, S. Park, S.-H. Lee, and Y. Endoh, Phys. Rev. Lett. **90**, 137004 (2003).
 - ⁵ N. P. Armitage, F. Ronning, D. H. Lu, C. Kim, A. Damascelli, K. M. Shen, D. L. Feng, H. Eisaki, Z.-X. Shen, P. K. Mang, N. Kaneko, M. Greven, Y. Onose, Y. Taguchi, and Y. Tokura, Phys. Rev. Lett. **88**, 257001 (2002).
 - ⁶ A. Damascelli, Z. Hussain, and Z.-X. Shen, Rev. Mod. Phys. **75**, 473 (2003).
 - ⁷ T. Yoshida, X. J. Zhou, T. Sasagawa, W. L. Yang, P. V. Bogdanov, A. Lanzara, Z. Hussain, T. Mizokawa, A. Fujimori, H. Eisaki, Z.-X. Shen, T. Kakeshita, and S. Uchida, Phys. Rev. Lett. **91**, 027001 (2003).
 - ⁸ T. Tohyama and S. Maekawa, Phys. Rev. B **49**, 3596 (1994).
 - ⁹ R. J. Gooding, K. J. E. Vos, and P. W. Leung, Phys. Rev. B **50**, 12866 (1994).
 - ¹⁰ T. Tohyama and S. Maekawa, Phys. Rev. B **64**, 212505 (2001); **67**, 092509 (2003).
 - ¹¹ T. K. Lee, C. M. Ho, and N. Nagaosa, Phys. Rev. Lett. **90**, 067001 (2003); W.-C. Lee, T. K. Lee, C.-M. Ho, and P. W. Leung, *ibid.*, **91**, 057001 (2003).
 - ¹² J.-X. Li, J. Zhang, and J. Luo, Phys. Rev. B **68**, 224503 (2003).
 - ¹³ T. Tohyama, Phys. Rev. B **70**, 174517 (2004).
 - ¹⁴ C. Kusko, R. S. Markiewicz, M. Lindroos, and A. Bansil, Phys. Rev. B **66**, 140513 (2002).
 - ¹⁵ H. Kusunose and T. M. Rice, Phys. Rev. Lett. **91**, 186407 (2003).
 - ¹⁶ B. Kyung, J.-S. Landry, A.-M. S. Tremblay, Phys. Rev. B **68**, 174502 (2003); D. Sénéchal and A.-M. S. Tremblay, Phys. Rev. Lett. **92**, 126401 (2004); B. Kyung, V. Hankevych, A.-M. Daré, and A.-M. S. Tremblay, *ibid.* **93**, 147004 (2004).
 - ¹⁷ Q. S. Yuan, Y. Chen, T. K. Lee, and C. S. Ting, Phys. Rev. B **69**, 214523 (2004).
 - ¹⁸ See, e.g., C. C. Tsuei and J. R. Kirtley, Rev. Mod. Phys. **72**, 969 (2000); A. Snezhko, R. Prozorov, D. D. Lawrie, R. W. Giannetta, J. Gauthier, J. Renaud, and P. Fournier, Phys. Rev. Lett. **92**, 157005 (2004) and references therein.
 - ¹⁹ F. Onufrieva and P. Pfeuty, Phys. Rev. Lett. **92**, 247003 (2004).
 - ²⁰ A similar formulation was given by J. R. Schrieffer, X. G. Wen, and S. C. Zhang, Phys. Rev. B **39**, 11663 (1989), for the pure Hubbard (t - U) model at zero temperature.
 - ²¹ J. P. Lu, Phys. Rev. Lett. **68**, 125 (1992).
 - ²² S. Wakimoto, H. Zhang, K. Yamada, I. Swainson, H. Kim, and R. J. Birgeneau, Phys. Rev. Lett. **92**, 217004 (2004).